Robust and High Performance Pressure Retarded Osmosis Hollow Fiber Membranes for Osmotic Power Generation

Gang Han and Tai-Shung Chung
Dept. of Chemical and Biomolecular Engineering, National University of Singapore, 10 Kent Ridge Crescent, Singapore117602

DOI 10.1002/aic.14342
Published online January 16, 2014 in Wiley Online Library (wileyonlinelibrary.com)

Novel fabrication perspectives have been demonstrated to molecularly construct robust hollow fiber membrane supports for high performance thin-film composite (TFC) pressure retarded osmosis (PRO) membranes. For the first time, we found that the desirable hollow fiber supports should possess high stretch resistance and acceptable ductility. The microstructure strength of the hollow fiber support may have more weights on overall robustness of the TFC PRO membranes than the apparent cross-section morphology. Effectively manipulating the kinetics of phase inversion during spinning by maneuvering bore fluid chemistry, and polymer solution composition is a promising method to tailor the strength of hollow fiber supports. Prestabilization of the TFC membranes at elevated lumen pressures can significantly improve their PRO performance. The newly developed TFC PRO hollow fiber membranes exhibit a power density as high as 16.5 W/m^2 and a very low specific reverse salt flux (J_s/J_w) of 0.015 mol/L at a hydraulic pressure of 15 bar using synthetic seawater brine (1.0 M NaCl) as the draw solution. © 2014 American Institute of Chemical Engineers *AIChE J*, 60: 1107–1119, 2014

Keywords: pressure retarded osmosis, thin-film composite, hollow fiber, membrane robustness, power density, reverse salt flux

Introduction

The rapid growth in energy demand and the depletion of fossil fuels have stimulated worldwide search for alternative and sustainable power sources.[1,2] Osmotic power harvested from the mixing of water streams with different salinities is an emerging renewable energy source with enormous potential.[3,4] With up to 0.70–0.75 kWh of energy released when 1 m^3 river water mixes with ocean, the global estimation of this renewable energy is 1600 TWh/year.[5,6] Much higher energy can be generated if the high salinity retentate of reverse osmosis (RO) plants is mixed with freshwater. Not only can it potentially lower the overall energy consumption for desalination, but also solve the problem of disposing RO retentate.[7] It is foreseen that osmotic energy has immense potential and will make significant contributions to the global power production.[4–9]

In principle, osmotic power can be generated via pressure retarded osmosis (PRO) process where a semipermeable membrane is placed between two solutions of different salinities.[9,10] Driven by the chemical potential gradient, water spontaneously permeates across the membrane from the feed of low-salinity to the saltwater of high-salinity (which is referred to as the draw solution thereafter). If the draw solution compartment has a fixed volume, its hydraulic pressure would increase rapidly due to the large water inflow, thus drives the hydroturbine and produces electricity.[8–11] Based on the prototype PRO plant built by Statkraft, the power density of the PRO membranes should be larger than 5 W/m^2 in order to be commercially viable.[5,8,11] However, studies have demonstrated that commercially available semipermeable membranes such as conventional RO and forward osmosis (FO) membranes do not performance well in pressurized PRO processes due to severe internal concentration polarization (ICP) or weak membrane strengths.[12–17] Ideal membranes for high pressure PRO processes should possess (1) a high water permeability in order to have a high water flux, (2) robust mechanical strength to withstand the complicated forces and stresses, (3) an effective salt rejection to maintain the osmotic driving force, and (4) a low structure parameter to minimize the ICP.[4,18–23]

Several important advancements have been made in flat-sheet and hollow fiber thin-film composite (TFC) membranes for PRO processes.[18–27] Zhang et al. and Li et al. improved the stability and permeability of flat-sheet TFC PRO membranes by modifying the physicochemical properties of the supports and post-treating the polyamide selective layer.[18,19] Han et al. developed novel flat-sheet TFC PRO membranes that exhibited a power density of 12 W/m^2 at 15 bar using 1 M NaCl and deionized (DI) water as feeds.[20] Song et al. fabricated flat-sheet TFC PRO membranes on nanofiber supports and showed a power density of 15.2 W/m^2 at 15.2 bar when 1.06 M NaCl and 0.9 mM NaCl were used as feeds.[24] However, flat-sheet PRO membranes have several unavoidable shortcomings.[25,28–32] They are easily deformed in high pressure PRO processes due to membrane-spacer interactions that may lead to severe salt leakage, structure parameter enhancement, and hydraulic pressure loss in the feed flow channel. Moreover, the shadow effects from the spacer in

Correspondence concerning this article should be addressed to T.-S. Chung at chencts@nus.edu.sg.

the feed channel further reduces the overall water flux and power density.[25,28] In contrast, the self-supported hollow fiber membranes are of great interest due to the spacer-free module fabrication. Not only could this minimize the membrane deformation owing to membrane-spacer interactions, but also eliminate the aforementioned extra energy loss in the feed flow channel of flat-sheet modules.

For TFC PRO hollow fiber membranes, Han et al. recently developed novel membranes that can withstand transmembrane pressures up to 16 bar and exhibit a peak power density as high as 14 W/m^2 using synthetic seawater brine (1.0 M NaCl) and DI water as feeds.[21] Chou et al. also reported one TFC PRO hollow fiber membrane that can achieve a power density of 20.9 W/m^2 at 15 bar using 1.0 M NaCl as the draw solution, but their salt reverse flux is relatively high.[23] Zhang et al. invented another TFC PRO hollow fiber membrane which can produce a maximum power density of 24.0 W/m^2 at 20.0 bar with a very low ratio of salt reverse flux to water flux (i.e., less than 1 g/L) using 1 M NaCl as the concentrated brine.[22] Despite of these impressive developments, the underlying fundamental science and engineering for the fabrication of highly robust TFC PRO hollow fiber membranes with superior performance have not been fully explored.

As a continuous effort in developing effective PRO membranes, the objectives of this study are to investigate the underlying science of fabricating high performance TFC PRO hollow fiber membranes with an inner selective layer and to particularly focus on how to molecularly construct highly robust hollow fiber supports. By manipulating the chemistry of polymer solutions and the kinetics of phase inversion processes, we would first design hollow fiber supports with different micromorphology and mechanical strengths. After conducting interfacial polymerization on these supports under the same conditions and testing the resultant TFC PRO membranes by various synthetic brines, we would aim to elucidate the relationship between the physicochemical properties of the hollow fiber supports and the transporting properties, robustness, and power density of the TFC PRO membranes. This fundamental study may provide pertinent insights of design strategies of hollow fiber supports for the fabrication of highly robust TFC PRO hollow fiber membranes for power generation.

Experimental

Materials and chemicals

Matrimid® 5218 purchased from Vantico was used as the polymer to fabricate the hollow fiber membrane support. N-methyl-2-pyrrolidone (NMP, >99.5%) and diethylene glycol (DEG, >99.0%) from Merck were utilized as the solvent and pore former in the membrane fabrication, respectively. A mixture of glycerol (Aik Moh Pains & Chemicals Pte., Singapore) and water (50/50 wt %) was used to post treat the as-spun hollow fibers. Polyethylene oxide and polyethylene glycol with different molecule weights were purchased from Sigma–Aldrich to characterize pore characteristics and molecular weight cutoff (MWCO) of the hollow fiber supports. Trimesoyl chloride (TMC, >98%) and *m*-phenylenediamine (MPD, >99%) were ordered from Sigma–Aldrich as monomers for the interfacial polymerization reaction. Sodium dodecyl sulphate (SDS, >97%, Fluka) and triethylamine (TEA, >99%, Sigma–Aldrich) were used as additives, whereas hexane (>99.9%, Fisher Chemicals) as the solvent for the interfacial polymerization. Sodium chloride (NaCl) was acquired from Merck and DI water was produced by a Milli-Q unit (Millipore) with a resistivity of 15 MΩ cm.

Fabrication of hollow fiber membrane supports

To fabricate desirable hollow fiber supports for the inner selective TFC PRO membranes, a spinning process consisting of a single-layer spinneret and a dual-bath coagulation technology was used to control the phase inversion and membrane morphology during fiber formation. The detailed experimental set up and spinning procedures were described elsewhere.[21,33] Table 1 summarizes the spinning parameters for the hollow fiber supports. After phase inversion, the membranes were soaked in a 50 wt % glycerol aqueous solution for 2 days and then dried in the air at room temperature (about 23°C). For module fabrication, the hollow fiber membranes were assembled into the module holder which consists of two Swagelok stainless steel male run tees connected by a perfluoroalkoxy tube with an effective length of 13.0 cm. Both ends were sealed with a slow cure epoxy resin (KS Bond EP231, Bondtec).

Interfacial polymerization of TFC PRO hollow fiber membranes

A polyamide selective skin was formed on the inner surface of the hollow fiber supports via interfacial polymerization between MPD and TMC.[34] In a typical interfacial polymerization, a 2 wt % MPD aqueous solution containing 0.5 wt % TEA and 0.1 wt % SDS was first fed into the lumen of hollow fibers for 5 min. The residual droplets of MPD were then removed by purging a sweeping air. A 0.15 wt % TMC hexane solution was subsequently brought into contact with the MPD saturated membrane inner surface for

Table 1. Spinning Conditions of Hollow Fiber Membrane Supports

	Spinning Code			
Spinning Parameter	HF-1	HF-2	HF-3	HF-4
Polymer dope solution (wt %)	18/17/65 Matrimid/DEG/NMP		16.9/17/65.3/0.8 Marimid/DEG/NMP/H_2O	
Solubility parameter δ (Mpa)$^{1/2}$	23.1		23.3	
Bore-fluid solution (wt %)	H_2O/NMP 70:30	H_2O/NMP/EG 40:30:30	H_2O/NMP 70:30	H_2O/NMP 50:50
Solubility parameter δ (Mpa)$^{1/2}$	40.3	34.9	40.3	35.3
Polymer dope flow rate (mL/min)	0.6	1.15	1.5	1.5
Bore-fluid flow rate (mL/min)	0.3	0.71	0.75	0.75
Air-gap length (cm)	3.0	1.5	2.0	2.0
Take-up speed (m/min)	1.0 (free fall)	2.1 (free fall)	2.5 (free fall)	2.5 (free fall)
External coagulants	IPA/water (60/40 wt %, $\delta = 33.2$ (Mpa)$^{1/2}$) then tap water ($\delta = 47.8$ (Mpa)$^{1/2}$) using dual bathes of coagulation			
Spinneret dimension (mm)	Single-layer spinneret (1.2-0.68-0.48)			
Spinning temperature (°C)	Ambient (23°C ± 2)			
Post treatment	40/60 wt % glycerol/water for 2 days			

3 min, leading to the formation of the polyamide skin. The resultant TFC hollow fiber membranes were rinsed with water and then stored in DI water before further characterizations.

Membrane morphology, porosity, and mechanical properties

Membrane morphology was observed by a field-emission scanning electron microscope (FESEM JEOL JSM-6700LV). Membrane porosity of the hollow fiber support was measured using a standard protocol described in our previous studies.[21,22] Fiber mechanical properties, such as tensile modulus, maximum tensile strength, and elongation at break were determined by an Instron tensiometer (Model 5542, Instron Corp.) in watery phase at room temperature. A constant elongation rate of 10 mm/min with a starting gauge length of 25 mm was applied. Each reported value was an average of at least 10 fibers.

Pure water permeability and pore characteristics of the hollow fiber supports

Pure water permeability (PWP) of the fabricated hollow fiber membrane support was measured using a lab-scale PRO setup. As the hollow fiber supports have an inner selective skin, the feed water was pumped into the lumen side and the permeation water was collected from the shell side. The feed water was kept at a constant flow rate of 0.1 L/min and the applied pressure in the lumen was increased to predefined values. The PWP in L/(m^2 h bar) (or LMH/bar) was calculated using the equation

$$\mathrm{PWP} = \frac{Q}{A_m \Delta P} \tag{1}$$

where Q is the water permeation volumetric flow rate (L/h), A_m is the effective filtration area (m^2), and ΔP is the transmembrane pressure drop (bar).

The pore size, pore-size distribution, and MWCO of the hollow fiber supports were measured by solute rejection experiments using neutral solutes made of polyethylene oxide or polyethylene glycol with a concentration of 200 ppm at 1 bar. The concentrations of the neutral solutes in the feed and permeate were measured via a total organic carbon analyzer (TOC ASI-5000A, Shimadzu, Japan). The measured feed (C_f) and permeate (C_p) concentrations were used to calculate the effective solute rejection coefficient R (%) as

$$R = \left(1 - \frac{C_p}{C_f}\right) \times 100\% \tag{2}$$

The relationship between solute Stokes diameter (d_s, nm) and molecular weight (M_w, g/mol) of the neutral solutes can be expressed as[35,36]

$$\text{For PEG}: d_s = 33.46 \times 10^{-12} \times M^{0.557} \tag{3}$$

$$\text{For PEO}: d_s = 20.88 \times 10^{-12} \times M^{0.587} \tag{4}$$

By plotting the solute rejection R vs. d_s on a log-normal probability paper, a straight line is yielded and the mean effective pore-size μ_p (diameter) is found at $R = 50\%$, and the geometric standard deviation σ_p is obtained as the ratio of d_s at $R = 84.13\%$ and $R = 50\%$. Then, the pore-size distribution of the membrane can be expressed as following

$$\frac{dR(d_p)}{dd_p} = \frac{1}{d_p \ln\sigma_p \sqrt{2\pi}} \exp\left[-\frac{(\ln d_p - \ln \mu_p)^2}{2(\ln \sigma_p)^2}\right] \tag{5}$$

Mass transport characteristics of the TFC PRO hollow fiber membranes

The intrinsic water permeability (A), salt rejection (R), and salt permeability (B) of the TFC hollow fiber membranes were characterized by testing the membranes under the RO mode via a lab-scale circulating filtration apparatus. The water permeability coefficient (A) was determined from the pure water permeation fluxes under a transmembrane hydraulic pressure of 1–2 bar. The salt rejection (R_s) to NaCl was obtained by determining the conductivity of the permeate and the feed solution using a feed of 200 ppm NaCl at 1 bar. The salt permeability coefficient (B) was then determined according to the solution-diffusion theory as follows[18–22]

$$\frac{1 - R_s}{R_s} = \frac{B}{A(\Delta P - \Delta\pi)} \tag{6}$$

where ΔP and $\Delta\pi$ are the pressure difference and osmotic pressure difference across the membrane, respectively.

The membrane structure parameters S of the TFC membranes were obtained via a method described in the previous studies.[21,22]

PRO experiments

The setup for cross-flow PRO experiments has been reported in our previous studies.[21,22] Each TFC hollow fiber membrane was first tested at zero hydraulic pressure ($\Delta P = 0$) to evaluate its FO performance. Then, the hydraulic pressure applied on the draw solution was increased to predefined values. At each pressure, the PRO test was continued for more than 30 min at room temperature (~23°C). The flow rate at the shell side was kept at 0.2 L/min, whereas the flow rate at the lumen side was kept at 0.1 L/min. A lower feed flow rate in the lumen side was used to minimize the pressure drop through the fiber. NaCl was used as the solute to prepare the draw solution and feed solution, as listed in Table 2. All the tests were carried out under the PRO mode,

Table 2. Summary of the Synthetic Water Sources for PRO Tests

Synthetic Water Source		NaCl Concentration	Osmotic Pressure[a] (bar)
Salt water (Draw solution)	Seawater brine	1.0 M	49.2
Fresh water (Feed solution)	Deionized water	0	0
	River water	10 mM	0.49
	Wastewater brine	40 mM	1.96

[a]The osmotic pressure was calculated with the van't Hoff equation.

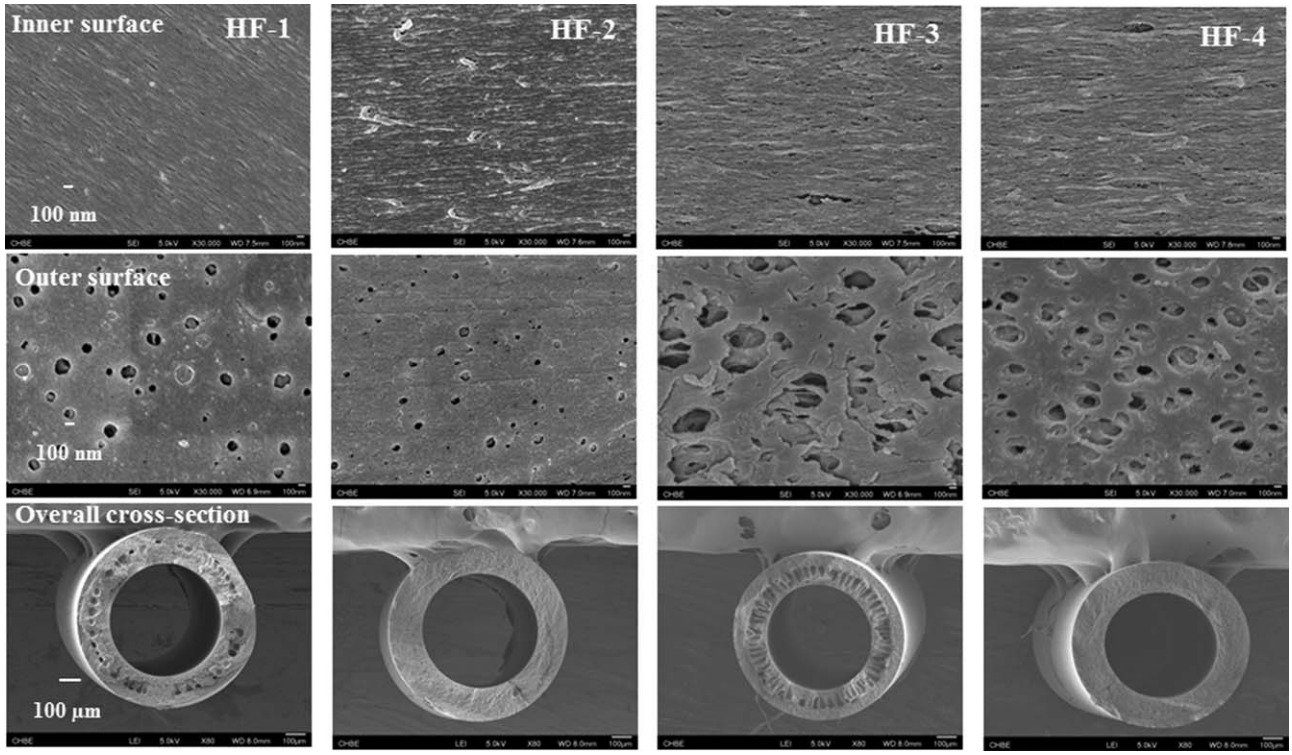

Figure 1. SEM micrographs of different bulk and surface morphologies of the newly developed hollow fiber supports.

where the selective layer of the membrane faces the draw solution. The water flux (J_w) was determined by measuring the weight change of the feed solution, and the reverse solute flux (J_s) was calculated via the change of conductivity with time in feed water.

In terms of energy production in PRO, the apparent osmotic power density (W) was calculated by the product of the transmembrane hydraulic pressure difference (ΔP) and the water permeation flux (J_w) across the membrane[19–22]

$$W = J_w \times \Delta P \tag{7}$$

W is a major performance indicator in PRO processes because it determines the required amount of membrane area and the size of the PRO plant for a given capacity of energy production.

Results and Discussion

Characteristics of the hollow fiber membrane supports

By using different polymer dope compositions and bore fluid chemistry, asymmetric hollow fiber supports with a relatively dense inner skin and a highly porous outer skin were designed. Figure 1 shows the inner surface, outer surface, and overall cross-section micrographs of the fabricated hollow fiber supports. To exclude the influences from fiber dimension, all hollow fiber supports were made to have a similar inner diameter ranging from 520 to 540 μm (Table 3). As all bore fluids have a high amount of nonsolvents, all inner surfaces exhibit relatively dense skins. This morphology is favorable for the formation of a less defective polyamide layer with a good water permeability during interfacial polymerization.[21–23,37] However, the order of inner surface porosity seems to follow HF-1 < HF-2 < HF-3 < HF-4 due to the following factors: (1) both HF-1 and HF-2 were spun from a dope with a higher polymer content than that of HF-3 and HF-4 (18 vs. 16.9 wt %); as a result, the former have tighter skins than the latter; (2) HF-4 was spun from a bore fluid containing the highest NMP. As the bore fluid has a relatively close solubility parameter with the polymer solution as shown in Table 1, it results in slightly delayed demixing and a relatively porous skin; (3) similarly, the bore fluid of HF-2 has a relatively close solubility parameter with the spinning dope because it contains a large percentage of ethylene glycol (EG) which is a viscous nonvolvent. Because isopropyl alcohol (IPA)/water (60/40) was used as the first external coagulant and has a faintly close solubility parameter with the spinning dope, all outer surfaces have disconnected large pores, which not only facilitates water and salt transport as well as reduces the ICP in the support layer, but also provides more robust mechanical strength than fully connected surface pores under stresses. In addition, the outer surface porosity follows the trend of HF-2 ≈ HF-

Table 3. Summary of the Porous Properties and Dimension of the Hollow Fiber Supports

Membrane ID	μ_p (nm)	σ_p	PWP [L/(m^2 bar h)]	MWCO (KDa)	Porosity (%)	Fiber OD/ID (μm)
HF-1	6.5 ± 0.2	1.50 ± 0.05	245.9 ± 15.0	32.8 ± 3.2	72.4 ± 3.5	880/520
HF-2	6.4 ± 0.5	1.36 ± 0.01	253.9 ± 54.6	25.3 ± 3.8	75.5 ± 2.4	860/540
HF-3	13.7 ± 0.5	1.47 ± 0.01	284.4 ± 58.2	146.4 ± 6.7	70.3 ± 1.8	820/520
HF-4	14.8 ± 0.9	1.43 ± 0.04	605.4 ± 38.8	157.3 ± 6.7	80.5 ± 2.7	840/520

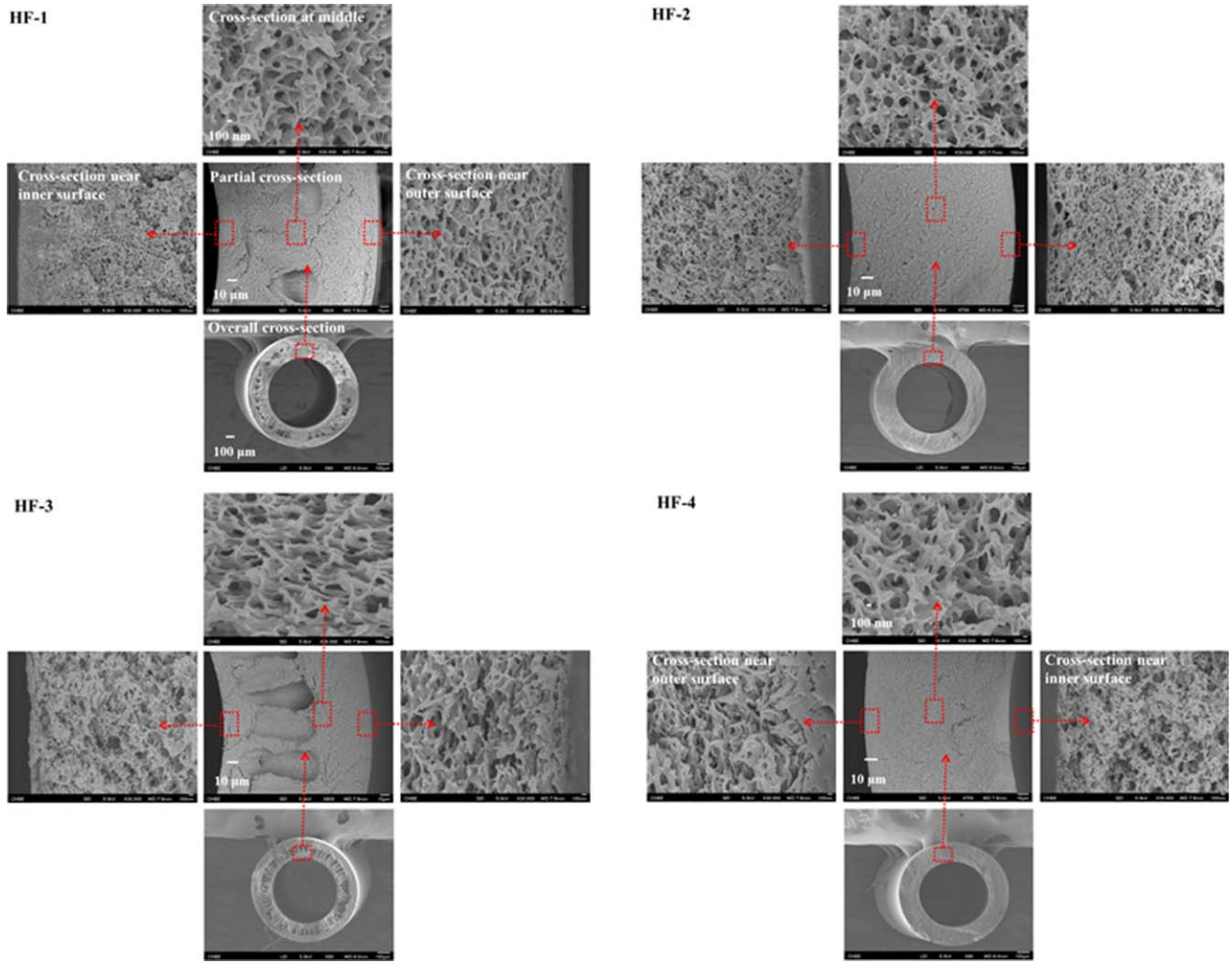

Figure 2. SEM micrographs of the cross-section morphology of the newly developed hollow fiber supports.

[Color figure can be viewed in the online issue, which is available at wileyonlinelibrary.com.]

1 < HF-4 ≈ HF-3 because the first two fibers were spun from a dope with a higher polymer content than the last two.

In addition, all hollow fibers show good concentricity but different overall cross-section morphology, as illustrated in Figure 2. When H_2O/NMP 70:30 was used as the bore fluid, small tear-shape macrovoids were produced in the middle of the cross-section of HF-1 and short finger-like macrovoids were formed in the inner cross-section of HF-3. In contrast, HF-2 and HF-4 have a fully sponge-like cross-section structure. These discrepancies in cross-section morphology are due to the fact that macrovoids are usually formed via instantaneous demixing between the polymer solution and bore fluid as well as bore fluid intrusion from the lumen of hollow fibers,[38] while sponge-like macrovoid-free morphology is often resulted from delayed demixing. As H_2O/NMP 70:30 is a much stronger coagulant than H_2O/NMP 50:50 and H_2O/NMP/EG 40:30:30 (i.e., solubility parameters of $\delta = 40.3$ vs. 35.3 and 34.9 $(Mpa)^{1/2}$, respectively), it results in membranes with macrovoids. Microscopically, all hollow fibers possess a porous open-cell structure across the membrane, which is essential to reduce transport resistance and minimize ICP. A relatively dense sponge-like layer can be observed beneath the inner skin of all hollow fibers. The microstructure of this layer plays an important role in determining the quality of the polyamide layer as well as the effectiveness of dissipating stresses across the membrane under high pressures.[21,22,27]

Table 3 presents the basic characteristics of the as-spun hollow fiber supports including the mean pore size, PWP, MWCO, and porosity. Figure 3 shows the pore-size distribution

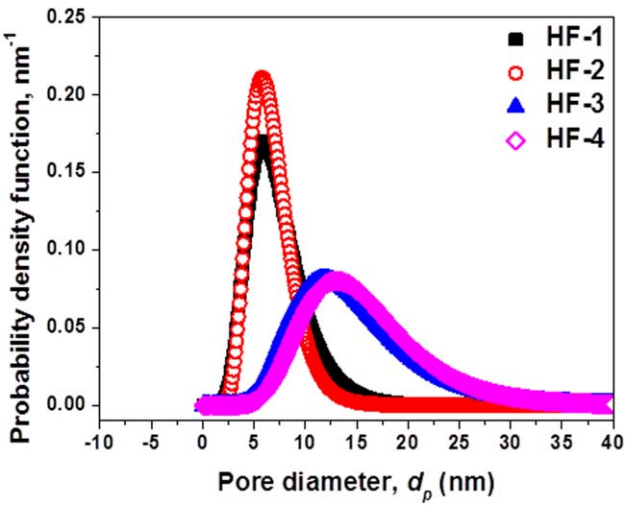

Figure 3. Pore-size distribution of the newly developed hollow fiber supports.

[Color figure can be viewed in the online issue, which is available at wileyonlinelibrary.com.]

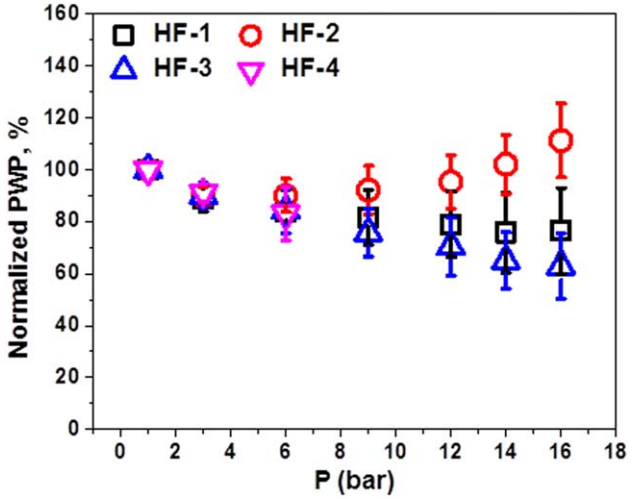

Figure 4. Variations of the normalized PWP as a function of hydraulic pressure difference across the newly developed hollow fiber supports.

[Color figure can be viewed in the online issue, which is available at wileyonlinelibrary.com.]

curves of the fibers. HF-1 and HF-2 have narrow pore-size distributions and close mean pore sizes of 6.5 and 6.4 nm, respectively; whereas HF-3 and HF-4 possess larger mean pore sizes of about 13.7 and 14.8 nm, respectively, with broader pore-size distributions. The MWCO follows a similar trend as their mean pore sizes. These differences are mainly resulted from dissimilar thermodynamics and kinetics during phase inversion due to different dope compositions and bore fluid chemistry. HF-1, HF-2, and HF-3 have similar overall porosity ranging from 70.3 to 75.5%, whereas HF-4 has a relative larger porosity of 80.5% because it was spun from a dope with lower polymer content and a bore fluid with a high NMP percentage. As a consequence, HF-4 shows a much larger PWP of 605 L/(m^2 bar h) compared to other fibers [245.9–284.4 L/(m^2 bar h)].

Due to the high pressure water flowing in the lumen, the TFC hollow fiber membranes would be compacted and expanded in PRO processes. As the mechanical stability of the supports under pressures determines the robustness of the final TFC PRO membranes,[18–22] the PWP of the hollow fiber supports at various transmembrane hydraulic pressures were studied using the PRO setup. As shown in Figure 4, the PWP of HF-1 and HF-3 rapidly decrease by 22 and 37%, respectively, with an increase in transmembrane pressure to 16 bar due to membrane compaction. In contrast, HF-2 first displays a slight reduction in PWP at low pressures ($\Delta P < 6$ bar) and then the PWP increases by 17% at 16 bar. This phenomenon is possibly due to membrane deformation such as increased membrane surface area, reduced thickness and defect formation under high pressures in the lumen because the microstructure formed by the EG containing bore fluid is less rigid. HF-4 was physically broken at 9 bar, while the burst pressures of HF-1, HF-2, and HF-3 are larger than 16 bar (Table 4). Clearly, the mechanical stability and physical responses of hollow fiber supports can be tailored via effectively controlling dope composition and phase inversion conditions. In addition, hollow fiber membranes with a fully sponge-like cross-section morphology do not always possess better robustness than those containing small size macrovoids as we originally thought.[19–22] The strength of membrane microstructure and the effectiveness of stress dissipation under PRO pressures may have more weights on overall membrane robustness than apparent cross-section morphology.

Table 4 summarizes the mechanical properties of the newly developed hollow fiber supports in terms of tensile modulus, tensile strength, and elongation at break. HF-3 shows the highest tensile modulus followed by HF-1 and then HF-4 and HF-2. In terms of tensile strength and elongation at break, the hollow fiber support follows the orders of HF-1 > HF-3 > HF-2 > HF-4 and HF-2 > HF-3 > HF-4 > HF-1, respectively. The membrane toughness was estimated by integrating the stress–strain curve. HF-2 has the largest toughness and followed by HF-3 and HF-1 and then HF-4. Consistent with the results from high pressure PRO tests, HF-1, HF-2, and HF-3 have burst pressures greater than 16 bar, which is much larger than 9 bar of HF-4.

Characteristics of the TFC PRO hollow fiber membranes

The water permeability A, salt rejection R, salt permeability B, and membrane structure parameter S of the fresh and stabilized TFC hollow fiber membranes are shown in Figure 5. The as-prepared TFC hollow fiber membranes have a water permeability ranging from 1.7 to 1.9 LMH/bar with a salt permeability of 0.15–0.48 LMH before stabilization. Under no-pressure PRO tests (when $\Delta P = 0$), they have water fluxes of 36.7–41.0 LMH and reverse salt fluxes of 10.2–11.0 gMH when 1 M NaCl is used as the draw solution and DI water as the feed, as shown in Table 5. In addition, they possess relative small structure parameters of lower than 810 μm (Figure 5).

Subsequently, the fresh TFC hollow fiber membranes were stabilized by progressively increasing the hydraulic pressure in the lumen to certain values, and then the transporting properties and structure parameters of the stabilized membranes were retested under same conditions. Experiments have shown that the precompression of TFC membranes can stabilize membrane's PRO performance,[19–22,24] and the stabilized pressures for TFC-HF1, TFC-HF2, TFC-HF3, and TFC-HF4 were 16, 15, 15, and 6 bar for 30 min, respectively. As shown in Figure 5, the water and salt permeability of TFC-HF1 increase from 1.9 to 3.6 LMH/bar and from 0.48 to 0.73 LMH, respectively, after stabilization at 16 bar. They are from 1.7 to 3.1 LMH/bar and 0.16 to 0.61 LMH,

Table 4. Summary of the Mechanical Properties of the Hollow Fiber Supports

Membrane ID	Tensile Modulus (MPa)	Tensile Strength (MPa)	Elongation at Break (%)	Toughness[a] ($\times 10^6$ J/m^3)	Burst Pressure (bar)
HF-1	299.6 ± 24.3	10.4 ± 1.0	22.0 ± 2.6	2.0 ± 0.3	>16
HF-2	148.3 ± 23.1	6.9 ± 0.5	51.0 ± 2.9	2.9 ± 0.4	>16
HF-3	326.1 ± 24.5	7.8 ± 0.4	36.2 ± 3.1	2.3 ± 0.8	>16
HF-4	190.4 ± 30.4	6.7 ± 0.4	34.8 ± 4.5	1.9 ± 0.7	≈9

[a]Toughness was calculated by taking the integral underneath the stress-strain curve.

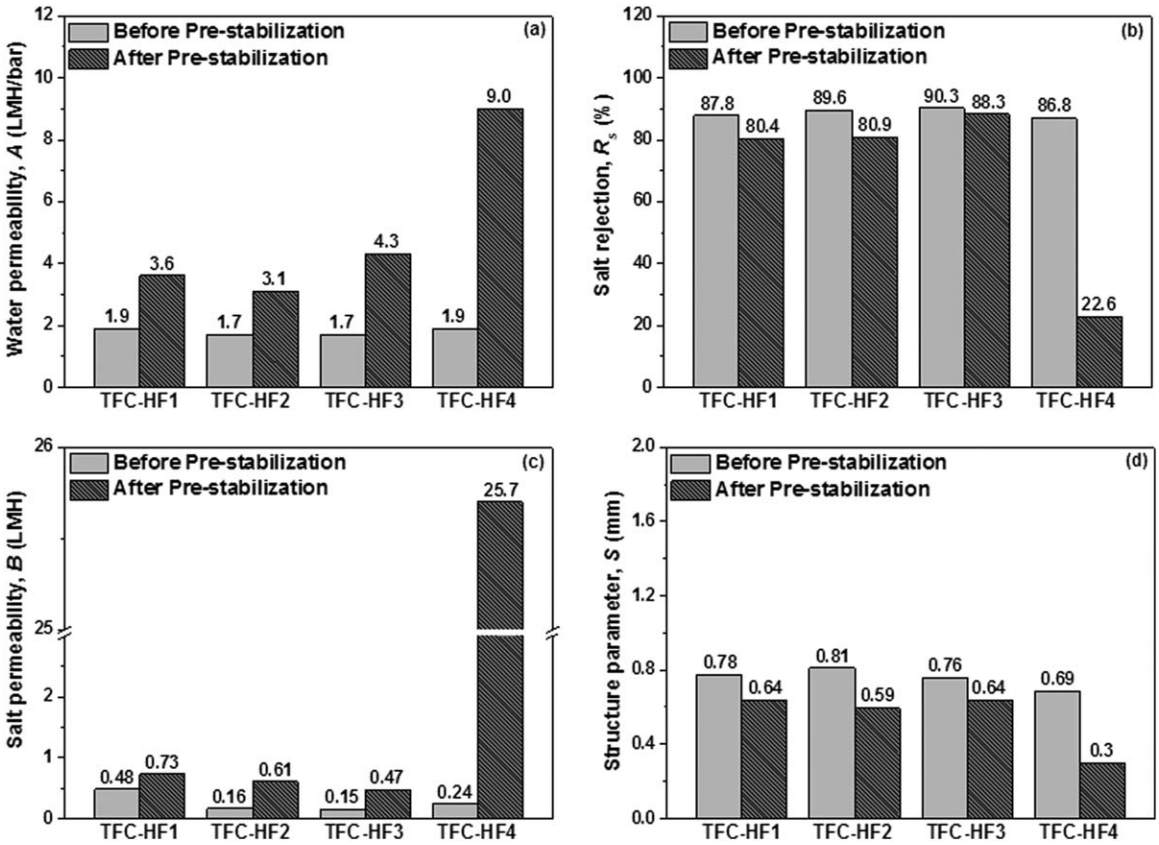

Figure 5. Transport properties of the developed TFC-HF1, TFC-HF2, THF-HF3, and TFC-HF4 membranes before and after being stabilized at 16, 15, 15, and 6 bar in PRO, respectively.

(a) Water permeability (*A*) tested at 1 bar, (b) salt rejection (*R*) tested at 1 bar with a 200 ppm NaCl feed, (c) salt permeability (*B*), and (d) structure parameter (*S*).

respectively, for TFC-HF2 and from 1.7 to 4.3 LMH/bar and 0.15 to 0.47 LMH, respectively, for TFC-HF3 after stabilization at 15 bar, and from 1.9 to 9.0 LMH/bar and 0.24 to 25.7 LMH, respectively, for TFC-HF4 after stabilization at 6 bar. In summary, the stabilized TFC hollow fiber membranes show great improvements in water flux with slightly increases in reverse salt flux except TFC-HF4. In addition, all stabilized membranes maintain good salt rejections of larger than 80% except TFC-HF4 which decreases to 23%. The dramatically increased salt permeability and decreased salt rejection of TFC-HF4 suggest that the polyamide selective layer is significantly deformed. Furthermore, the structure parameters of all TFC hollow fiber membranes decrease after the stabilization process. As membrane structure parameter is defined as $S = t\tau/\varepsilon$ where t, τ, and ε are the thickness, tortuosity, and porosity of the support layer, a lower S not only indicates that the supporter layer becomes thinner, but also implies that porosity increases and tortuosity decreases because of the stretch around the hoop direction by the applied hydraulic pressure in the lumen. A low S helps reduce the ICP effects, thus the stabilized TFC hollow fiber membranes may show improvements on power density.

Table 5. FO Performance of the TFC Hollow Fiber Membranes Before and After Stabilization

	FO Performance (PRO mode)	
Membrane ID	Water Flux (LMH)	Reverse Salt Flux (gMH)
TFC-HF1	**38.3 ± 2.7**	**10.6 ± 1.7**
Stabilized @ 16 bar	42.8 ± 3.0	15.5 ± 3.2
TFC-HF2	**36.7 ± 2.3**	**10.4 ± 2.4**
Stabilized @ 15 bar	45.6 ± 4.1	10.5 ± 3.6
TFC-HF3	**39.2 ± 2.1**	**10.2 ± 1.6**
Stabilized @ 15 bar	48.2 ± 3.2	10.5 ± 3.2
TFC-HF4	**41.0 ± 2.4**	**11.0 ± 3.3**
Stabilized @ 6 bar	48.5 ± 3.2	30.5 ± 6.4

Draw solution: 1 M NaCl; feed solution: deionized water; Flow rate: lumen side is 0.1 L/min; shell side is 0.2 L/min.

Figure 6 shows the surface and cross-section morphology of the stabilized TFC PRO hollow fiber membranes. A typical "ridge-and-valley" morphology with a layer thickness of 162.4–178.5 nm is formed on the lumen surface. The leaf-like polyamide layers of TFC-HF3 and TFC-HF4 have a relative bigger leaf comparing to TFC-HF1 and TFC-HF2 because the supports of the former have larger pores than the latter.[34,37]

PRO performance of the TFC hollow fiber membranes

The PRO performance of the newly developed TFC hollow fiber membranes were evaluated via a lab-scale PRO setup using synthetic seawater brine (1 M NaCl) as the draw solution, DI water, synthetic river water (10 mM NaCl), and wastewater brine (40 mM NaCl) as the freshwater streams (Table 2).

Figure 7 shows the water fluxes (J_w) at various hydraulic pressures before and after stabilization, using synthetic seawater brine as the draw solution and DI water as the feed. Before stabilization, the water flux of TFC-HF1 decreases

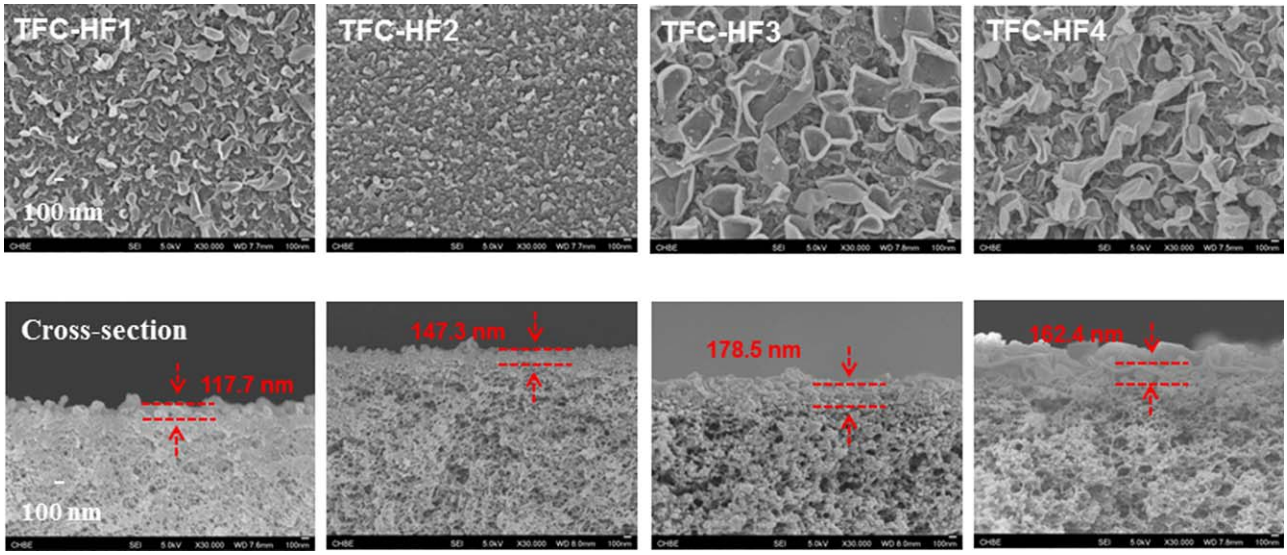

Figure 6. Typical morphology of the stabilized TFC-PRO hollow fiber membranes.

[Color figure can be viewed in the online issue, which is available at wileyonlinelibrary.com.]

with an increase in pressure before 9 bar and then maintains almost the same value at 9–16 bar. The water flux of TFC-HF2 displays a similar trend before 9 bar but increases at higher pressures of 9–15 bar. For TFC-HF3, the water flux first shows a reduction at low pressures of 0–6 bar, remains the same value at 6–12 bar, and then slowly increases with elevating pressure to 15 bar. The water flux of TFC-HF4 exhibits a similar trend at low pressures but experiments end at 6 bar because of weak fiber properties. Figure 7 also shows the water flux after stabilization which is very stable

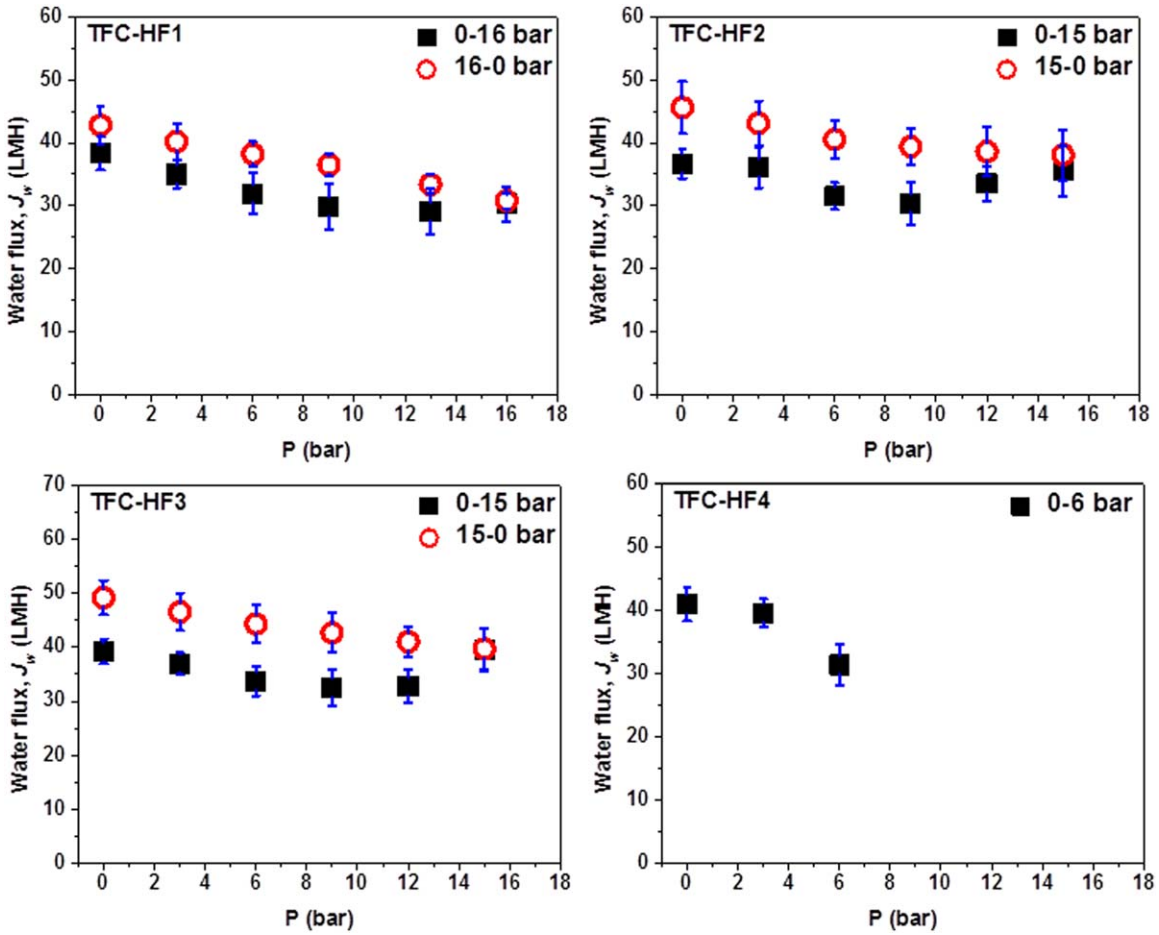

Figure 7. Water flux (J_w) of the newly developed TFC hollow fiber membranes at various hydraulic pressure differences before and after stabilization.

[Color figure can be viewed in the online issue, which is available at wileyonlinelibrary.com.]

and slowly decreases with increasing hydraulic pressure. Interestingly, the stabilization process significantly increases the water flux. However, different degrees of flux increments are observed for different fibers. TFC-HF2 and TFC-HF3 have larger flux improvements than TFC-HF1 because their support structures are more adjustable than the TFC-HF1 during the stabilization process. TFC-HF2 has a less rigid structure because EG was used in its bore fluid, while TFC-HF3 was spun from a dope with a lower polymer concentration. Because membrane power density is a product of water flux and transmembrane hydraulic pressure, the power density of these TFC hollow fibers is almost proportional to their water fluxes with a power density up to 13.7–16.5 W/m^2 at a hydraulic pressure of 15–16 bar, as illustrated in Figure 8. Particularly, the TFC-HF3 membrane exhibits the highest W of 16.5 W/m^2 at 15 bar, which is attributed to its overall superior mechanical properties (Table 4) and high water flux (Figure 5 and Table 5).

Figure 9 shows the specific reverse salt flux (J_s/J_w) as a function of pressure before and after stabilization. A large specific reverse salt flux is unacceptable because it will directly reduce the driving force and elevate ICP, thus greatly decreases the module's productivity in real PRO applications. TFC-HF1 shows a very small specific salt flux of 0.28 g/L at 0 bar, then the specific salt flux slowly reaches 0.6 g/L at 9 bar and rapidly increases to 1.9 g/L (or 0.032 mol/L) at 16 bar. The specific salt flux of TFC-HF2 is relative small at low pressures, such as 0.23 and 0.37 g/L at 0 and 3 bar, respectively. Then, the specific salt flux increases to 2.2 g/L (0.038 mol/L) at 15 bar. Interestingly, TFC-HF3 always possesses a relative low specific salt flux of less than 0.9 g/L (0.015 mol/L) in the whole pressure range from 0 to 15 bar. The slow increment in salt flux with pressure indicates the good membrane stability. To the best of our knowledge, this PRO performance in terms of high power density and low salt reverse flux outperforms most PRO membranes reported in the literatures.[3,13,21–23] TFC-HF4 possesses the worst rejection stability with a specific salt flux of 4.2 g/L (0.07 mol/L) only at 6 bar. In addition, the specific salt fluxes of the stabilized TFC hollow fiber membranes show minor changes comparing to those before stabilization, which suggests that the selectivity of the polyamide layer is maintained and no significant defects are formed even at high pressures. Clearly, stabilization enhances water permeability and decrease membrane structure parameter of the TFC hollow fiber membranes without accompanying severe salt leakage, resulting in high PRO performance.

As the TFC hollow fibers with an inner selective layer undergoes stretch in the radial direction in response to the applied hydraulic pressure in the lumen, it affects the free volume, permeability, and selectivity of the polyamide layer as well as the support layer. When the hydraulic pressure is low, the stretch is elastic and the membrane selectivity is not

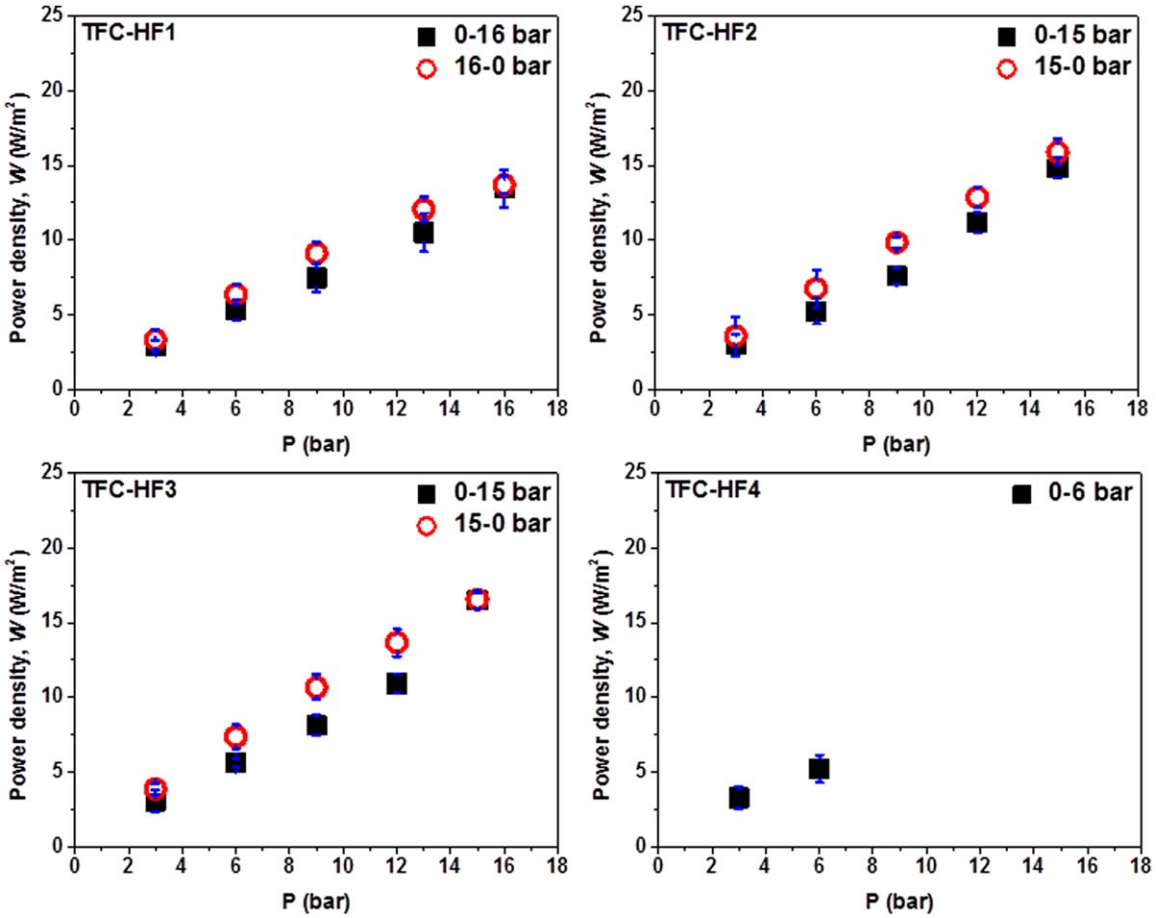

Figure 8. Experimental power density (W) of the newly developed TFC hollow fiber membranes at various hydraulic pressure differences before and after stabilization.

[Color figure can be viewed in the online issue, which is available at wileyonlinelibrary.com.]

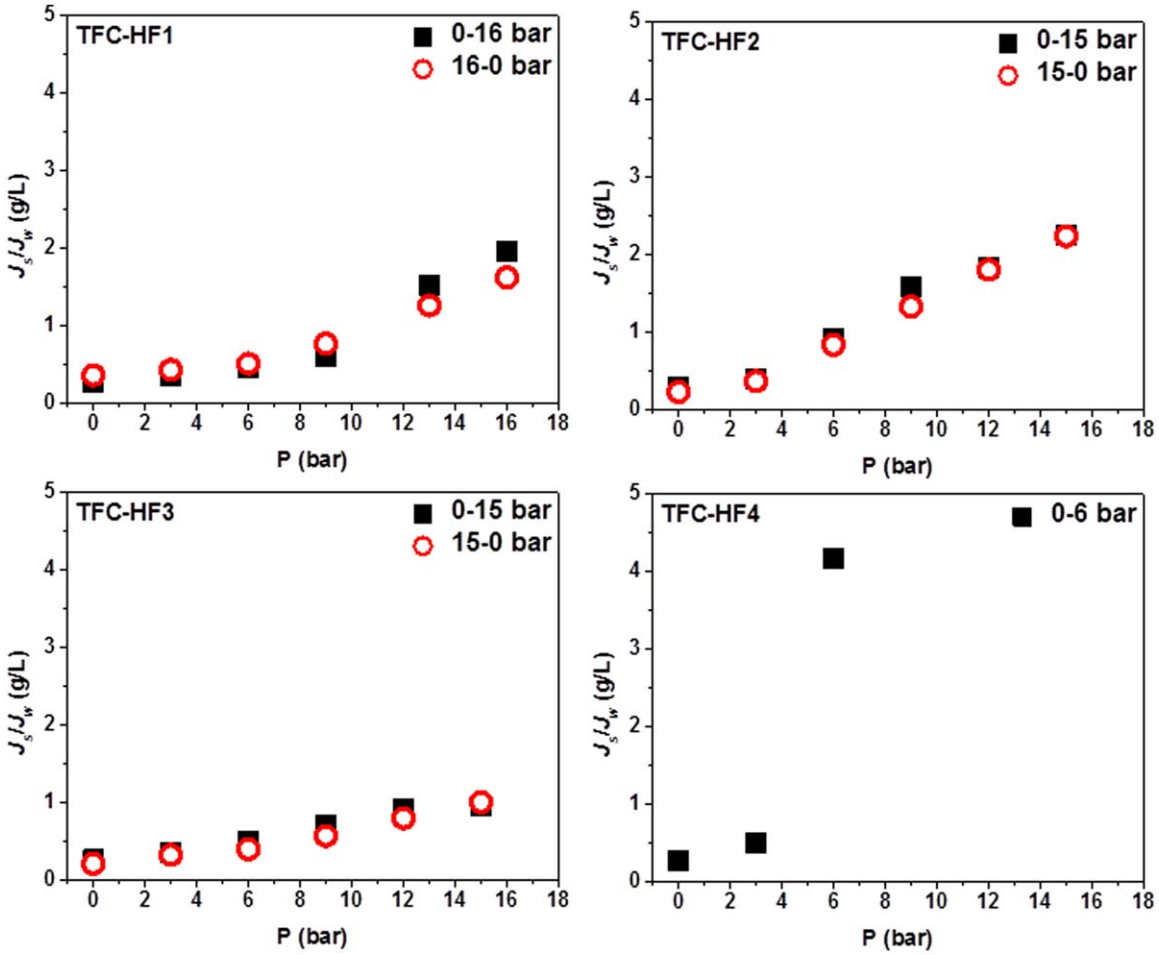

Figure 9. Specific salt flux (J_s/J_w) of the newly developed TFC hollow fiber membranes at various hydraulic pressure differences before and after stabilization.

[Color figure can be viewed in the online issue, which is available at wileyonlinelibrary.com.]

affected. Once the pressure increases to a certain value, the support layer may suffer dramatically physical changes and the polyamide layer may detach from and/or rupture the support, resulting in a dramatically increase in reverse salt flux. The stability of TFC hollow fiber membranes under pressures is therefore strongly dependent on the robustness of their supports. Figure 10 illustrates the stress–strain curves of the developed hollow fibers and three distinct kinds of fibers can be identified. One fiber that has high stretch resistance (tensile stress) but low ductility (elongation at break) is named as "strong fiber." This type of fiber normally possesses high rigidity and is stable at low pressures and shows a slow increase in salt reverse flux with elevated pressures. However, the reverse salt flux will increase rapidly once the applied pressure beyond a certain value (such as >9 bar for TFC-HF1 in Figure 9). In contrast, one fiber that has high ductility but relatively low stretch resistance is called "ductile fiber." The reverse salt flux of this fiber will increase significantly with increasing lumen pressure even at a relative low pressure (such as >3 bar for TFC-HF2 in Figure 9). The other kind of fiber is the "tough fiber" which not only has a relatively high stretch resistance but also a good ductility. The reverse salt flux of the "tough fiber" can be maintained at a relative low level even at high pressures (such as TFC-HF3 in Figure 9). Fibers with poor tensile strength and ductility are normally very weak and possess low burst pressures such as 9 bar for HF-4. A comparison among Figures 7–10 suggests that a proper balance between the membrane stretch resistance and ductility is very important for the overall stability of inner selective TFC PRO hollow fiber membranes.

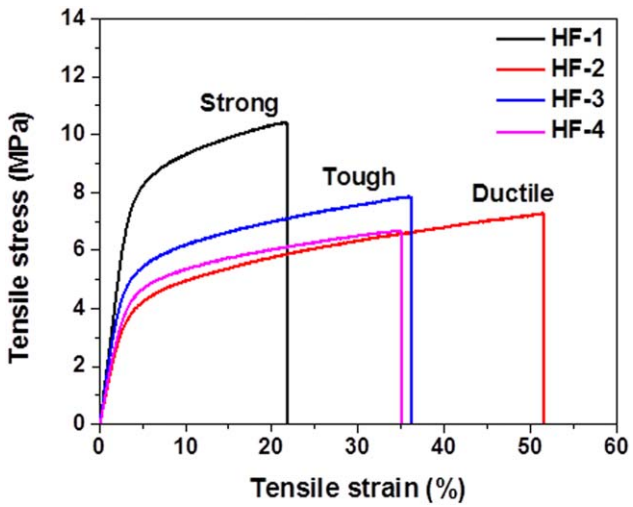

Figure 10. Typical stress–strain curves of the newly developed hollow fibers.

[Color figure can be viewed in the online issue, which is available at wileyonlinelibrary.com.]

It seems that the TFC PRO hollow fiber membranes with a fully sponge-like morphology do not always possess better mechanical robustness than those with small macrovoids, the overall membrane strength may not only depend on the overall cross-section morphology, but also rely on the micropolymer network within the membrane. If the sponge-like layer near the inner surface is strong enough to uniformly distribute the external forces from the lumen pressure and dissipate the stresses, the small centered macrovoids may not play a determining role to weaken the overall PRO performance. An effective hollow fiber support with desirable microstructure for TFC PRO hollow fiber membranes can be obtained by effectively controlling the phase inversion process, particularly the interactions between polymer solution and bore fluid.

As the newly developed TFC-HF3 membranes have the highest water flux and lowest reverse salt flux even at high pressures. Their PRO performance were further evaluated using synthetic seawater brine, and synthetic river water (10 mM NaCl) and wastewater (40 mM NaCl) as feeds, respectively. Figure 11 shows the water permeation flux and power density at various hydraulic pressures. The water flux decreases slightly with an increase in feed water salinity. As a result, the power density drops from 16.5 to 14.4 and to 10.6 W/m^2 at 15 bar when the feed water is changed from DI water to the synthetic river water and wastewater brine, respectively. These reductions are mainly attributed to the combinative effects of the reduced osmotic pressure difference and enhanced ICP effects due to higher salt concentrations in feed water.[20–23,39,40] Nevertheless, the newly developed TFC PRO hollow fiber membranes have an encouraging power density with an impressive low specific salt flux for PRO power generation applications.[41–45]

Conclusions

By effectively controlling the phase separation process during spinning, we have demonstrated the science and engineering of fabricating robust hollow fiber supports for inner-selective high performance TFC PRO membranes for osmotic power generation. The following conclusions can be further drawn from this work:

1. The newly developed TFC hollow fiber membranes display a power density as high as 16.5 and 14.4 W/m^2 at 15 bar using DI water and synthetic river water as the feeds, respectively, and synthetic seawater brine as the salty water. Meanwhile, a very low specific reverse salt flux of 0.9 g/L (or 0.015 mol/L) was achieved even at 15 bar.
2. The mechanical properties together with the membrane morphology of the hollow fiber support play significant roles in the robustness and PRO performance of the TFC hollow fiber membranes. A robust hollow fiber support for inner selective TFC PRO hollow fiber membranes

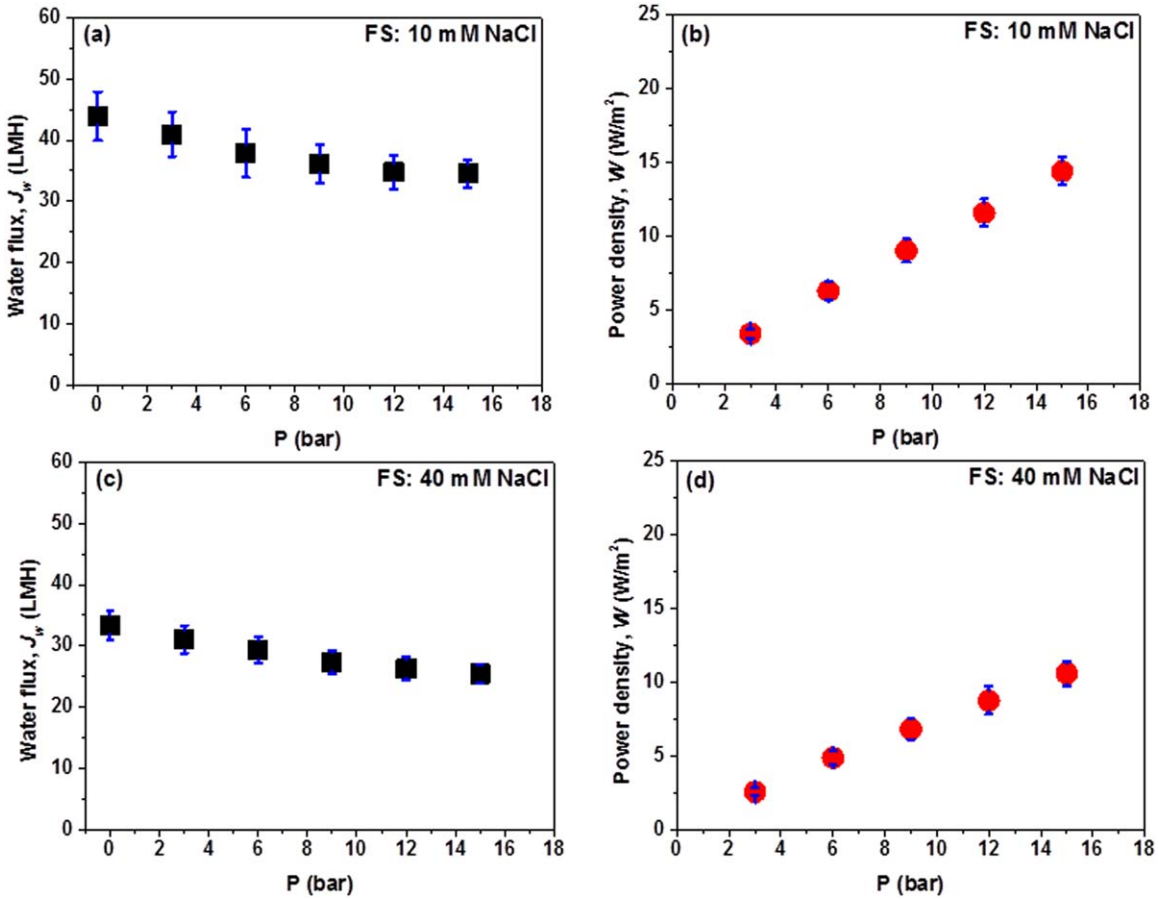

Figure 11. PRO performance of the stabilized TFC-HF3 hollow fiber membranes at various transmembrane hydraulic pressures (1 M NaCl solution was used as the draw solution, 10 mM and 40 mM NaCl were used as the feed water).

[Color figure can be viewed in the online issue, which is available at wileyonlinelibrary.com.]

may have both high stretch resistance and ductile capacity. The microstructure strength of the hollow fiber support and the effectiveness of stress dissipation under pressures may determine the overall membrane robustness more than the apparent cross-section morphology. Effectively manipulating phase separation kinetics during spinning using proper bore fluids and polymer solutions is a promising strategy to maximize the strength of the hollow fiber support.

3. Prestabilization of the inner selective TFC hollow fiber membranes with high robustness not only can significantly improve membrane water permeability and decrease membrane structure parameter, but also enhance PRO performance. The current study may have valuable implications for the fabrication of effective TFC PRO hollow fiber membranes for osmotic power generation.

Acknowledgments

This research grant is supported by the Singapore National Research Foundation under its Environmental & Water Technologies Strategic Research Programme and administered by the Environment & Water Industry Programme Office (EWI) of the PUB under the project entitled "Membrane development for osmotic power generation, Part 1. Materials development and membrane fabrication" (1102-IRIS-11-01) and NUS grant number of R-279-000-381-279.

Notation

A = water permeability, L/(m^2 h bar)
B = salt permeability, L/(m^2 h)
C_f = feed concentration, mol/L
C_p = permeate concentration, mol/L
C = salt concentration, mol/L
D = solute diffusion coefficient, m^2/s
J_s = reverse salt flux, g/(m^2 h)
J_w = water flux, L/(m^2 h)
W = power density in PRO, W/m
ΔP = pressure across the membrane, bar
R_s = solute rejection
S_t = membrane structural parameter, m
π = osmotic pressure, bar
σ = geometric standard deviation
d_p = pore diameter, nm
d_s = solute diameter, nm
δ = solubility parameter, δ
LMH = L/m^2·h

Literature Cited

1. Chu S, Majumdar A. Opportunities and challenges for a sustainable energy future. *Nature*. 2012;488:294–303.
2. Evans A, Strezov V, Evans TJ. Assessment of sustainability indicators for renewable energy technologies. *Renew Sustain Energy Rev*. 2009;13:1082–1088.
3. Zhao S, Zou L, Tang CY, Mulcahy D. Recent developments in forward osmosis: opportunities and challenges. *J Membr Sci*. 2012;396:1–21.
4. Chung TS, Li X, Ong RC, Ge Q, Wang H, Han. G. Emerging forward osmosis (FO) technologies and challenges ahead for clean water and clean energy applications. *Curr Opin Chem Eng*. 2012;1:246–257.
5. Gerstandt K, Peinemann KV, Skilhagen SE, Thorsen T, Holt T. Membrane processes in energy supply for an osmotic power plant. *Desalination*. 2008;224:64–70.
6. Logan BE, Elimelech M. Membrane-based processes for sustainable power generation using water. *Nature*. 2012;488:313–319.
7. Chung TS, Zhang S, Wang KY, Su JC, Ling MM. Forward osmosis processes: yesterday, today and tomorrow. *Desalination*. 2012;287:78–81.
8. Skilhagen SE, Dugstad JE, Aaberg RJ. Osmotic power—power production based on the osmotic pressure difference between waters with varying salt gradients. *Desalination*. 2008;220:476–482.
9. Loeb S. Production of energy from concentrated brines by pressure-retarded osmosis: I. Preliminary technical and economic correlations. *J Membr Sci*. 1976;1:49–63.
10. Loeb S, Norman RS. Osmotic power plants. *Science*. 1975;189:654–655.
11. Thorsen T, Holt T. The potential for power production from salinity gradients by pressure retarded osmosis. *J Membr Sci*. 2009;335:103–110.
12. Mehta GD, Loeb S. Performance of permasep B-9 and B-10 membranes in various osmotic regions and at high osmotic pressures. *J Membr Sci*. 1979;4:335–349.
13. Loeb S, Hessen FV, Shahaf D. Production of energy from concentrated brines by pressure retarded osmosis. II. Experimental results and projected energy costs. *J Membr Sci*. 1976;1:249–269.
14. Lee KL, Baker RW, Lonsdale HK. Membranes for power generation by pressure-retarded osmosis. *J Membr Sci*. 1981;8:141–171.
15. Achilli A, Childress AE. Pressure retarded osmosis: from the vision of Sidney Loeb to the first prototype installation—review. *Desalination*. 2010;261:205–211.
16. Yip NY, Tiraferri A, Phillip WA, Schiffman JD, Hoover LA, Kim YC, Elimelech M. Thin-film composite pressure retarded osmosis membranes for sustainable power generation from salinity gradients. *Environ Sci Technol*. 2011;45:4360–4369.
17. Chou S, Wang R, Shi L, She Q, Tang CY, Fane AG. Thin-film composite hollow fiber membranes for pressure retarded (PRO) process with high power density. *J Membr Sci*. 2012;389:25–33.
18. Zhang S, Fu FJ, Chung TS. Substrate modifications and alcohol treatment on thin film composite membranes for osmotic power. *Chem Eng Sci*. 2013;87:40–50.
19. Li X, Zhang S, Fu FJ, Chung TS. Deformation and reinforcement of thin-film composite (TFC) polyamide-imide (PAI) membranes for osmotic power generation. *J Membr Sci*. 2013;434:204–217.
20. Han G, Zhang S, Li X, Chung TS. High performance thin film composite pressure retarded osmosis (PRO) membranes for renewable salinity-gradient energy generation. *J Membr Sci*. 2013;440:108–121.
21. Han G, Wang P, Chung T.S. Highly robust thin-film composite pressure retarded osmosis (PRO) hollow fiber membranes with high power densities for renewable salinity-gradient energy generation. *Environ Sci Technol*. 2013;47:8070–8077.
22. Zhang S, Chung TS. Minimizing the instant and accumulative effects of salt permeability to sustain ultrahigh osmotic power density. *Environ Sci Technol*. 2013;47:10085–10092.
23. Chou S, Wang R, Fane AG. Robust and high performance hollow fiber membranes for energy harvesting from salinity gradients by pressure retarded osmosis. *J Membr Sci*. 2013;448:44–54.
24. Song X, Liu Z, Sun DD. Energy recovery from concentrated seawater brine by thin-film nanofiber composite pressure retarded osmosis membranes with high power density. *Environ Sci Technol*. 2013;6:1199–1210.
25. She Q, Jin X, Tang CY. Osmotic power production from salinity gradient resource by pressure retarded osmosis: effects of operating conditions and reverse solute diffusion. *J Membr Sci*. 2012;401–402:262–273.
26. Huang L, Bui N, Meyering MT, Hamlin TJ, McCutcheon JR. Novel hydrophilic Nylon 6,6 microfiltration membrane supported thin film composite membranes for engineered osmosis. *J Membr Sci*. 2013;437:141–149.
27. Bui NN, McCutcheon JR. Hydrophilic nanofibers as new supports for thin film composite membranes for engineered osmosis. *Environ Sci Technol*. 2013;47:1761–1769.
28. Kim YC, Elimelech M. Adverse impact of feed channel spacers on the performance of pressure retarded osmosis. *Environ Sci Technol*. 2012;46:4673–4681.
29. Sivertsen E, Holt T, Thelin W, Brekke G. Pressure retarded osmosis efficiency for different hollow fibre membrane module flow configurations. *Desalination*. 2013;312:107–123.
30. Park M, Kim JH. Numerical analysis of spacer impacts on forward osmosis membrane process using concentration polarization index. *J Membr Sci*. 2013;15:10–20.
31. Kim YC, Kim Y, Oh D, Lee KH. Experimental investigation of a spiral-wound pressure-retarded osmosis membrane module for osmotic power generation. *Environ Sci Technol*. 2013;47:2966–2973.
32. Sivertsen E, Holt T, Thelin W, Brekke G. Modelling mass transport in hollow fibre membranes used for pressure retarded osmosis. *J Membr Sci*. 2012;417–418:69–79.

33. Widjojo N, Chung TS, Krantz WB. A morphological and structural study of ultem/P84 copolyimide dual-layer hollow fiber membranes with delamination-free morphology. *J Membr Sci*. 2007;294:132–146.
34. Cadotte JE. Reverse osmosis membrane. US Patent 4039440, 1977.
35. Han G, Zhang S, Li X, Widjojo N, Chung TS. Thin film composite forward osmosis membranes based on polydopamine modified polysulfone substrates with enhancements in both water flux and salt rejection. *Chem Eng Sci*. 2012;80:219–231.
36. Singh S, Khulbe KC, Matsuura T, Ramamurthy P. Membrane characterization by solute transport and atomic force microscopy. *J Membr Sci*. 1998;142:111–127.
37. Li X, Wang KY, Helmer B, Chung TS. Thin-film composite membranes and formation mechanism of thin-film layers on hydrophilic cellulose acetate propionate substrates for forward osmosis processes. *Ind Eng Chem Res*. 2012;51:10039–10050.
38. Widjojo N, Chung TS. The thickness and air-gap dependence of macrovoid evolution in phase-inversion asymmetric hollow fiber membranes. *Ind Eng Chem Res*. 2006;45:7618–7626.
39. Zhao S, Zou L. Relating solution physicochemical properties to internal concentration polarization in forward osmosis. *J Membr Sci*. 2011;379:459–467.
40. Mehta GD, Loeb S. Internal polarization in the porous substructure of a semipermeable membrane under pressure-retarded osmosis. *J Membr Sci*. 1978;4:261–265.
41. Thorsen T, Holt T. WO Patent 047733 A1, 2003.
42. Thorsen T, Holt T. US Patent 7,566,402 B2, 2009.
43. Thorsen T, Holt T. US Patent 0008330 A1, 2009.
44. Alsvik IL, Hägg MB. Pressure retarded osmosis and forward osmosis membranes: materials and methods. *Polymers* 2013;5:303–327.
45. Fu FJ, Zhang S, Sun SP, Wang KY, Chung TS. POSS-containing delamination-free dual-layer hollow fiber membranes for forward osmosis and osmotic power generation. *J Membr Sci*. 2013;443:144–155.

Manuscript received Oct. 10, 2013, and revision received Dec. 17, 2013.